Spurious velocities in the steady flow of an incompressible fluid subjected to external forces [1]

J.-F. Gerbeau, C. Le Bris
ENPC-CERMICS, La Courtine 93167 Noisy-Le-Grand Cedex, France

M. Bercovier
The Hebrew University of Jerusalem, Israel

Abstract

We show that a non physical velocity may appear in the numerical computation of the flow of an incompressible fluid subjected to external forces. A distorted mesh as well as the use of a numerical method which does not rigorously ensure the incompressibility condition turn out to be responsible for this phenomenon. We illustrate it with numerical examples and we propose a projection method which improves the results.

Résumé

Nous montrons qu'un champ de vitesse sans signification physique peut apparaître dans la simulation numérique d'un fluide incompressible soumis à des forces extérieures. Un maillage déformé ainsi que l'utilisation d'une méthode n'assurant pas rigoureusement la condition d'incompressibilité s'avèrent être à l'origine de ce phénomène. Nous l'illustrons au travers d' exemples numériques et nous proposons une méthode de projection qui améliore les résultats.

We are interested here in the steady state of one incompressible homogeneous fluid in presence of a body force. This force may result from a coupling (*e.g.* magnetohydrodynamic equations or Boussinesq equations) or may be a given external force. For the sake of simplicity we shall only consider here this latter case.

When this force is the gradient of a potential, namely $\mathbf{f} = \nabla\Phi$, and when the velocity obeys to the no-slip condition on the boundary of a fixed domain, we expect to obtain a fluid everywhere at rest. But, as will be seen, numerical simulations which do not ensure rigorously $\operatorname{div} \mathbf{u} = 0$ may lead to a non-zero velocity.

[1]Work partially supported by PECHINEY, Direction des Recherches et Développements, France.

We give a few examples of this phenomenon in Section 1 and we propose a first explanation in Section 2. The deformation of the mesh plays a role in the observed inaccuracies, but it is not their unique cause.

With a general force ($\mathbf{f} = \mathbf{curl}\ g + \nabla\Phi$), we have noticed that the "gradient part" may also produce a velocity field which pollutes the physical flow. We give an example of such a fact in Subsection 1.4. For the practical applications, it is worth noticing that this phenomenon may *a fortiori* induce important numerical errors in coupled problems.

Section 3 is devoted to a projection method which eliminates the spurious speeds when $\mathbf{f} = \nabla\Phi$ (this method could easily be extended to the case of a force $\mathbf{f} = \nabla\Phi + \mathbf{curl}\ g$ when Φ is *a priori* known). In Section 4, we extend this method in order to reduce the inaccuracy for any $\mathbf{f}$ whose decomposition is not *a priori* known.

Let us note that a method close to ours has already been suggested by O. Besson *et al.* in [1] for a penalty formulation for the pressure. Nevertheless, our presentation allows us to establish a link between the spurious speeds and the deformation of the grid (*cf.* Appendix A). More precisely, we explain why spurious speeds do not appear on a right mesh with some peculiar forces, and we also show that they do appear with some forces even on a right mesh. Moreover, we give an error estimate (*cf.* Appendix B) which proves that our method improves the results on any meshes.

The numerical simulations are performed with the FEM code FIDAP[2] Version 7.52 and with a home-made code. We use the pairs Q1/P0 and Q2/P1 of finite elements spaces to approximate the velocity and the pressure. It is well-known that the pair Q1/P0 does not rigorously satisfy the Ladyzenskaia-Babuska-Brezzi condition and yields a spurious pressure (see V. Girault and P.-A. Raviart [2] or M.D. Gunzburger [3] for instance). Nevertheless, the problem presented here is independent of this fact and occurs also with the elements Q2/P1 which satisfy the LBB condition.

1 Some numerical experiments

1.1 A free surface problem

Our initial motivation was to improve a 2D free surface algorithm. Two incompressible fluids separated by an interface are subjected to a force $f = \nabla\Phi_0$, with $\Phi_0(x, y) = \frac{5}{2}y^2 - 10x$. Their densities are 2300 kg/m^3 and 2150 kg/m^3, their viscosity 1.1 m^2/s and 2.5 m^2/s. We solve the Navier-Stokes

[2]FIDAP is a trademark of Fluid Dynamics International, Inc.

equations in a box with homogeneous Dirichlet boundary conditions on three sides and $\mathbf{u}.\mathbf{n} = 0$ on the fourth side. The steady state interface is a curve $\Phi(x, y) = C$ where C is a constant determined by the conservation of the volume. The theoretical velocity is zero. Numerically, the position of the interface is good but we notice the apparition of a vortex (0.2 m/s) in each fluid (figure 1).

In order to understand the problem raised above, we simplify the experiment : in the three following tests, we just consider one fluid in a closed box Ω with various given forces and we solve the linear Stokes equations :

$$-\eta \triangle \mathbf{u} + \nabla p = \rho \mathbf{f} \quad \text{on } \Omega \tag{1}$$

$$\operatorname{div} \mathbf{u} = 0 \quad \text{on } \Omega \tag{2}$$

$$\mathbf{u} = 0 \quad \text{on } \partial\Omega \tag{3}$$

We set η=0.01 m^2/s and ρ=1 kg/m^3 in the sequel.

1.2 One fluid subjected to a constant force f

We assume $\mathbf{f}$ is constant and equal to $(100, 100)$ on Ω. In Figure 2, we use Q1/P0 elements and we see that no velocity appears on a right grid (maximum about 0.1e-11 m/s) whereas the velocity reaches 0.83 m/s on bent elements. In Figure 3, very similar results are obtained with Q2/P1 elements.

This suggests that the deformation of the grid plays a role in the inaccuracy on the velocity, and may explain the difficulty mentioned in Section 1.1 in the case of a free surface (where elements are bent since the mesh follows the interface in our computation).

1.3 One fluid subjected to a force $\mathbf{f} = \nabla\Phi$

In this test, we use Q1/P0 element and the force $\mathbf{f}$ is equal to $\nabla\Phi_1$ with $\Phi_1(x, y) = x^5 + x^4y^3 + x^2y + y^4$. The right hand side of Figure 4 shows that spurious speeds appear on a bent mesh (maximum : 0.19e-1 m/s) but one may see on the left hand side that they also appear on a grid whose elements are squares (maximum : 0.76e-3m/s). Therefore, the deformation of the mesh makes clearly worse the accuracy on the velocity, but imprecise results may also appear on rectangular elements.

Similar results were obtained with Q2/P1 elements.

1.4 One fluid subjected to a force $\mathbf{f} = \nabla\Phi + \mathbf{curl}\ g$

The two previous tests deal with a fluid at rest. We now build an experiment where the force is the sum of a gradient part and a solenoidal part, thereby creating a non-zero velocity :

$$f = \nabla\Phi + \mathbf{curl}\ g. \tag{4}$$

In order to enforce the incompressibility and the no-slip condition on the boundary, we set $g = g_0$ with g_0 built as follows :

$$\begin{aligned} A &= k[xy(H-x)(W-y)]^2, && (5)\\ \mathbf{u} &= \mathbf{curl}\ A, && (6)\\ g_0 &= \mathbf{curl}\ \mathbf{u}, && (7) \end{aligned}$$

where H and W are respectively the height and the width of the 2D box and k is a constant. For the numerical computations, $H = W = 1$, $k = 0.1$ and $\Phi(x,y) = \Phi_0(x,y) = \frac{5}{2}y^2 - 10x$.

Note that the velocity $\mathbf{u}$ can be analytically computed with (6) and $p = \Phi$ (up to an additive constant).

Figure 5 shows the velocity field on a mesh with rectangular elements (left hand side) and a comparison between the theoretical first component of the velocity and the numerical one on the straight line $y = 0.4$ of Ω : the result is very precise (it is difficult to distinguish the two curves). The same test computed on a distorted mesh is presented in Figure 6 with Q1/P0 elements and in Figure 7 with Q2/P1 elements : the flow is perturbated in the both cases.

Remark 1.1 It is worth noticing that, when $\Phi = 0$ (i.e. the force is divergence free), the numerical velocity is very close to the theoretical one both on rectangular and bent elements. Thus the deformation of the grid seems to affect the velocity essentially in presence of a non divergence free force.

1.5 Other experiments

Let us briefly mention other experiments which lead to analogous conclusions.

The flow $\mathbf{u}$ defined by (6) is the solution of the *Navier-Stokes* equations for the force $\mathbf{f} = \nabla\Phi_0 + \mathbf{curl}\ g_0 + \mathbf{u}.\nabla\mathbf{u}$. If we compute the numerical solution in this nonlinear setting, we observe that spurious velocities appear again on a bent mesh.

Likewise, they appear in many other experiments that we do not detail here and that involve other boundary conditions, a three dimensional box, a transient flow.

Let us also notice that the inaccuracy seems to increase with the Reynolds number and to decrease with the typical size of the mesh.

2 An attempt of explanation

Let us recall first of all why the fluid is at rest in presence of $\mathbf{f} = \nabla\Phi$.

For $m \geq 0$, we denote as usual by $H^m(\Omega)$ as the Sobolev space

$$H^m(\Omega) = \{u \in L^2(\Omega); D^\gamma u \in L^2(\Omega), \forall\gamma, |\gamma| \leq m\}$$

where $\gamma = (\gamma_1, \gamma_2, \gamma_3)$ is a multi-index and $|\gamma| = \gamma_1 + \gamma_2 + \gamma_3$. For $m \geq 1$, $H_0^m(\Omega)$ is the subspace of $H^m(\Omega)$ consisting of functions vanishing on $\partial\Omega$. We denote by $L_0^2(\Omega)$ the space

$$L_0^2(\Omega) = \{q \in L^2(\Omega); \int_\Omega q\,dx = 0\}$$

We shall suppose in the sequel that $\mathbf{f} \in L^2(\Omega)^2$. The Stokes problem (1)-(3) may be formulated in a variational form : to find $\mathbf{u} \in H_0^1(\Omega)^2$ and $p \in L_0^2(\Omega)$ such that

$$\left\{ \begin{array}{rcl} \eta \int_\Omega \nabla\mathbf{u}.\nabla\mathbf{v}\,dxdy - \int_\Omega p\mathrm{div}\,\mathbf{v}\,dxdy & = & \int_\Omega \mathbf{f}.\mathbf{v}\,dxdy \\ \int_\Omega q\mathrm{div}\,\mathbf{u}\,dxdy & = & 0 \end{array} \right. \tag{8}$$

for all $\mathbf{v} \in H_0^1(\Omega)^2$ and $q \in L_0^2(\Omega)$.

In particular, taking $\mathbf{v} = \mathbf{u}$, we have :

$$\eta \int_\Omega |\nabla\mathbf{u}|^2\,dxdy = \int_\Omega \mathbf{f}.\mathbf{u}\,dx = \int_\Omega \nabla\Phi.\mathbf{u}\,dx = -\int_\Omega \Phi\mathrm{div}\,\mathbf{u}\,dxdy = 0, \tag{9}$$

which shows that $\mathbf{u} = 0$ almost everywhere in Ω, i.e. the fluid is at rest.

Let us notice that the crucial point of this proof is that $\mathrm{div}\,\mathbf{u} = 0$ or, more precisely, that $\nabla\Phi$ is orthogonal (in $L^2(\Omega)$) to $\mathbf{u}$ as soon as $\mathrm{div}\,\mathbf{u} = 0$ in Ω and $\mathbf{u}.\mathbf{n} = 0$ on $\partial\Omega$. As we recall hereafter, this property does not hold for the discrete problem.

Following the presentation of V. Girault and P.-A. Raviart [2], we introduce for each $h > 0$, W_h and Q_h two finite-dimensional spaces such that

$W_h \subset H^1(\Omega)^2$ and $Q_h \subset L^2(\Omega)$. The latter is assumed to contain the constant functions. We set :

$$X_h = W_h \cap H_0^1(\Omega)^2 = \{\mathbf{v}_h \in W_h; \mathbf{v}_h|_{\partial\Omega} = 0\},$$

$$M_h = Q_h \cap L_0^2(\Omega) = \left\{ q_h \in Q_h; \int_\Omega q_h \, dx = 0 \right\}.$$

The variational problem (8) is then approximated by : find $\mathbf{u}_h \in X_h$ and $p_h \in M_h$ such that

$$\left\{ \begin{aligned} \eta \int_\Omega \nabla \mathbf{u}_h . \nabla \mathbf{v}_h \, dxdy - \int_\Omega p_h \mathrm{div}\, \mathbf{v}_h \, dxdy &= \int_\Omega \mathbf{f} . \mathbf{v}_h \, dxdy \\ \int_\Omega q_h \mathrm{div}\, \mathbf{u}_h \, dxdy &= 0 \end{aligned} \right. \tag{10}$$

for all $\mathbf{v}_h \in X_h$ and $q_h \in M_h$. In the case of $\mathbf{f} = \nabla\Phi$, we obtain as in the continuous case :

$$\int_\Omega |\nabla \mathbf{u}_h|^2 \, dx = -\frac{1}{\eta} \int_\Omega \Phi \mathrm{div}\, \mathbf{u}_h \, dx \tag{11}$$

but now the right hand side of (11) is not necessarily zero since Φ does not belong to M_h in general. Thus, the approximated velocity is not zero, which may explain the inaccuracies observed in the numerical computations of Subsections 1.1, 1.2 and 1.3. Moreover, equation (11) shows that the approximated velocity increases when the viscosity η decreases which has been noticed in the experiments.

Let us note that the above considerations do not explain the influence of the grid. Distorted elements are known to produce inaccuracies (see [4]) but we are unfortunately not able to derive here a precise error estimate linking the spurious speeds together with the deformation of the mesh.

Nevertheless, we propose now a way to avoid spurious velocities when $\mathbf{f} = \nabla\Phi$ which will enable us to understand why some results are much better on rectangular elements (at least with some potentials).

3 A method to avoid spurious speeds when $\mathbf{f} = \nabla\Phi$

In the following developments, we shall suppose, without loss of generality, that $\int_\Omega \Phi \, dx = 0$. The potentials Φ_0 and Φ_1 of the previous section can easily be changed to satisfy this property.

In order to obtain a zero velocity field when $\mathbf{f} = \nabla\Phi$, we suggest the following projection method :

First step : We compute $\Pi_h\Phi$, the orthogonal projection in $L^2(\Omega)$ of Φ onto M_h. In other words, we search $\Pi_h\Phi \in M_h$ such that :

$$\int_\Omega \Pi_h \Phi q_h \, dx = \int_\Omega \Phi q_h \, dx \tag{12}$$

for all $q_h \in M_h$.

Second step : We replace (10) by this alternative formulation of the Stokes problem : find $\mathbf{u}_h \in X_h$ and $p \in M_h$ such that

$$\left\{ \begin{array}{rcl} \eta \int_\Omega \nabla \mathbf{u}_h . \nabla \mathbf{v}_h \, dxdy - \int_\Omega p_h \mathrm{div}\, \mathbf{v}_h \, dxdy & = & -\int_\Omega \Pi_h \Phi \mathrm{div}\, \mathbf{v}_h \, dxdy \\ \int_\Omega q_h \mathrm{div}\, \mathbf{u}_h \, dxdy & = & 0 \end{array} \right. \tag{13}$$

for all $\mathbf{v}_h \in X_h$ and $q \in M_h$.

Thus we have

$$\int_\Omega |\nabla \mathbf{u}_h|^2 \, dx = -\frac{1}{\eta} \int_\Omega \Pi_h \Phi \mathrm{div}\, \mathbf{u}_h \, dx = 0 \tag{14}$$

since $\Pi_h \Phi \in M_h$. Therefore $\mathbf{u}_h = 0$.

We have tested this method (with a home-made code) in the experiments of Subsections 1.2 and 1.3 : the spurious velocities disappear both on a rectangular and a distorted mesh (see Table 1 for Q1/P0 elements and Table 2 for Q2/P1 elements).

We are now able to explain why spurious speeds do not appear on rectangular elements with the potentials Φ_0 and Φ_1 of experiments 1.2 and 1.4, at least for the Q1/P0 pair of finite elements spaces. For this purpose, let us compare

$$\int_\Omega \mathbf{f}.\mathbf{v}_j \, dx = -\int_\Omega \Phi \mathrm{div}\, \mathbf{v}_j \, dx$$

with

$$-\int_\Omega \Pi_h \Phi \mathrm{div}\, \mathbf{v}_j \, dx$$

where $\mathbf{v}_j$ denotes the velocity shape function (Q1) relative to the node j. Let us consider the four elements T_k, $k = 1, .., 4$ around the node j (see Figure 9). When the elements are *identical rectangles* whose sides are parallel to the coordinates axes, we establish in Appendix A that these two integrals are equal, for each j, whenever the following property holds :

$$\left\{\begin{array}{ll}\displaystyle\sum_{k=1}^{4}(-1)^k\int_{T_k}(x-x_k^c)\Phi(x,y)\,dxdy & =0\\ \displaystyle\sum_{k=1}^{4}(-1)^k\int_{T_k}(y-y_k^c)\Phi(x,y)\,dxdy & =0\end{array}\right. \tag{15}$$

where (x_k^c, y_k^c) are the coordinates of the center C_k of T_k.

In particular, (15) holds for any $\Phi(x,y) = \Psi_1(x)+\Psi_2(y)+\beta(x,y)$, where Ψ_1 and Ψ_2 denote two arbitrary functions and β is an arbitrary bilinear application.

Thus, on rectangular elements, for potentials of the above form, it is equivalent to implement $\int_\Omega \mathbf{f}.\mathbf{v}_j\,dx$ or $-\int_\Omega \Pi_h\Phi \mathrm{div}\,\mathbf{v}_j\,dx$ with the Q1/P0 elements. Therefore, in this particular cases, the traditional system (8) leads to the same calculus as the system (13) (which yields zero velocities, as proved above). This explains the good results obtained on a rectangular mesh for a simple force like in experiment 1.2. On the contrary, the potential $\Phi_1(x,y) = x^5+x^4y^3+x^2y+y^4$ of the experiments 1.3 does not satisfy (15), and we indeed check that it yields a wrong velocity even on rectangular elements.

In the case of gravity, no spurious speeds appear on a right grid with the Q2/P1 elements, since the potential of the force belongs to the pressure space. Note that it is no longer true on a distorted mesh.

4 Extension to the general case

The method presented in the previous section leads to very good results when $\mathbf{f}$ is the gradient of a known potential Φ. It can be straightforwardly extended to the case $\mathbf{f} = \nabla\Phi + \mathbf{curl}\; g$ when Φ and g are given.

The purpose of this last section is to extend this method to treat the case of any force $\mathbf{f}$ whose decomposition in a gradient and a solenoidal part is unknown.

First step : Let Y_h be a finite dimensional space such that $Y_h \subset H^1(\Omega)$ (in practice, we can take $Y_h = X_h$). We solve the following problem in order to compute an approximated gradient part of $\mathbf{f}$: find $\Phi_h \in Y_h$ such that

$$\int_\Omega \nabla\Phi_h.\nabla\psi_h\,dx = \int_\Omega \mathbf{f}.\nabla\psi_h\,dx \tag{16}$$

for all $\psi_h \in Y_h$.

Second step : We compute $\Pi_h \Phi_h \in M_h$ such that :

$$\int_\Omega \Pi_h \Phi_h q_h \, dx = \int_\Omega \Phi_h q_h \, dx \tag{17}$$

for all $q_h \in M_h$.

Third step : Finally, we solve the Stokes problem as follows : find $\mathbf{u}_h \in X_h$ and $p \in M_h$ such that

$$\left\{ \begin{array}{rcl} \eta \displaystyle\int_\Omega \nabla \mathbf{u}_h . \nabla \mathbf{v}_h \, dxdy - \int_\Omega p_h \mathrm{div}\, \mathbf{v}_h \, dxdy & = & \displaystyle\int_\Omega (\mathbf{f} - \nabla \Phi_h). \mathbf{v}_h \, dx \\ & & \displaystyle - \int_\Omega \Pi_h \Phi_h \mathrm{div}\, \mathbf{v}_h \, dxdy \\ \displaystyle\int_\Omega q_h \mathrm{div}\, \mathbf{u}_h \, dxdy & = & 0 \end{array} \right. \tag{18}$$

for all $\mathbf{v}_h \in X_h$ and $q_h \in M_h$.

Remark 4.1 Note that $Y_h \subset H^1(\Omega)$ (in practice Φ_h is approximated in the same space as the velocity), thus the calculus of $\nabla \Phi_h$ is consistent.

Remark 4.2 When $\mathrm{div}\, \mathbf{f} \in L^2(\Omega)$, the problem solved in the first step is the approximated variational formulation of

$$\left\{ \begin{array}{rcll} \triangle \Phi & = & \mathrm{div}\, \mathbf{f} & \text{on } \Omega \\ \dfrac{\partial \Phi}{\partial \mathbf{n}} & = & \mathbf{f}.\mathbf{n} & \text{on } \partial\Omega. \end{array} \right.$$

Let us check what happened when $\mathbf{f} = \nabla \Phi$. We recall that the method of Section 3 yields a zero velocity field. Unfortunately, it is not the case here. More precisely we have :

$$\int_\Omega |\nabla \mathbf{u}_h|^2 \, dx = \frac{1}{\eta} \int_\Omega (\mathbf{f} - \nabla \Phi_h). \mathbf{u}_h \, dx \tag{19}$$

Nevertheless, we prove in Appendix B that this estimate is better than (11) and the numerical results show hereafter that this method actually improves the accuracy in the experiments 1.2, 1.3 and 1.4.

Tables 3 and 4 show the results obtained when $\mathbf{f} = \nabla \Phi$ (but of course Φ is not *a priori* known) with Q1/P0 and Q2/P1 elements. Note that they are less precise than with the method of section 3 (especially for experiment 1.3) but still better than with the classical method.

Figure 8 and shows the results obtained with the force $\mathbf{f} = \mathbf{curl}\ \ g_0 + \nabla\Phi_0$ of experiment 1.4 on a distorted mesh (with g_0 and Φ_0 not *a priori* known by the code). Note that the computed velocity is very close to the theoretical one whereas the classical method gives a very bad flow on the same mesh (Figure 6 and 7). As previous, elements Q2/P1 and elements Q1/P0 give similar results (though Q2/P1 is of course slightly better).

Tables 5 and 6 show the dependence of $||\mathbf{u}_h||_{L^2(\Omega)^2}$ with h in the case $\mathbf{f} = \nabla\Phi_1$ on rectangular elements. In the case of Q1/P0 elements (resp. Q2/P1), the numerical experiment shows that, when the classical method is used, $||\mathbf{u}_h||_{L^2(\Omega)^2}$ decreases proportionally to h^2 (resp. h^4) whereas it decreases proportionally to h^4 (resp. h^6) with the projection method.

With an arbitrary potential Φ, we show rigorously in Appendix B that, with the Q1/P0 elements, $||\mathbf{u}_h||_{L^2(\Omega)^2}$ decreases at least proportionally to h with the classical method and proportionally to h^2 with the projection method.

5 Conclusion

It has been shown that spurious speeds can appear in the flow of a incompressible fluid subjected to external forces if the numerical velocity is not rigorously divergence free. We have proposed a method which completely cancels the spurious field for a force whose gradient part is *a priori* known, and which improves the results when the gradient part is unknown. A mathematical study of the method has been presented. This method has been tested with the Q1/P0 and Q2/P1 pairs of finite elements, but it can easily be extended to other pairs of elements.

We have also shown that no spurious field appears with a peculiar set of forces on a mesh composed of Q1/P0 rectangular elements. This explains the good results obtained on regular meshes with some simple forces like gravity. Nevertheless, it has been shown that spurious speeds may still appear on a regular mesh. Moreover, as soon as the mesh is composed of distorted elements, very inaccurate results may occur even with gravity. In all these cases, the method that we have proposed improves significantly the results.

References

[1] O. Besson, J. Bourgeois, P.A. Chevalier, J. Rappaz, and R. Touzani. Numerical modelling of electromagnetic casting processes. *Jour. Comp. Phys.*, 92(2):482–507, 1991.

[2] V. Girault and P.-A. Raviart. *Finite element methods for Navier-Stokes equations*. Springer-Verlag, 1986.

[3] M.D. Gunzburger. *Finite element methods for viscous incompressible flows : a guide to theory, practice, and algorithms*. Academic Press, 1989.

[4] J.M. Leone and P.M. Gresho. Another attempt to overcome the bent element blues. In *5th international conference on finite element methods in water ressources, Burlington*, pages 667–683. Springer-Verlag, 1984.

Appendix A

In this appendix, we use the Q1/P0 pair of finite element spaces to approximate the velocity and the pressure.

A.1. Notations

We shall denote by T_{ref} the reference unit square $[0,1]\times[0,1]$, by F_k the bilinear mapping that maps T_{ref} onto any quadrilateral T_k. F_k is defined by

$$F_k(\xi,\eta) = (x,y) = (A_0^k + A_1^k\xi + A_2^k\eta + A_3^k\xi\eta, B_0^k + B_1^k\xi + B_2^k\eta + B_3^k\xi\eta) \quad (20)$$

Denoting by (a_i^k, b_i^k) the coordinates of the vertices of T_k (*cf.* Figure 10), we have

$$\begin{cases} A_0^k = a_1^k, & A_1^k = a_2^k - a_1^k, \quad A_2^k = a_4^k - a_1^k, \quad A_3^k = a_3^k - a_2^k - a_4^k + a_1^k \\ B_0^k = b_1^k, & B_1^k = b_2^k - b_1^k, \quad B_2^k = b_4^k - b_1^k, \quad B_3^k = b_3^k - b_2^k - b_4^k + b_1^k. \end{cases}$$

The determinant of the Jacobian matrix of the transformation is

$$J^k(\xi,\eta) = A_1^kB_2^k - A_2^kB_1^k + (A_1^kB_3^k - A_3^kB_1^k)\xi + (A_3^kB_2^k - A_2^kB_3^k)\eta.$$

If $|T_k|$ denotes the area of T_k, let us remark that $J^k(\xi,\eta) = |T_k|$ as soon as T_k is parallelogram. The shape functions λ_i of the reference element are defined by

$$\begin{cases} \lambda_1(\xi,\eta) &= (1-\xi)(1-\eta) \\ \lambda_2(\xi,\eta) &= \xi(1-\eta) \\ \lambda_3(\xi,\eta) &= \xi\eta \\ \lambda_4(\xi,\eta) &= (1-\xi)\eta \end{cases}$$

The shape functions ψ_i^k of T_k are defined by :

$$\lambda_i = \psi_i^k \circ F^k.$$

One easily checks that :

$$\int_{T_k} \frac{\partial \psi_i^k}{\partial x}\,dxdy = \int_{T_{ref}} \left[(B_2 + B_3\xi)\frac{\partial\lambda_i}{\partial\xi} - (B_1 + B_3\eta)\frac{\partial\lambda_i}{\partial\eta}\right] d\xi d\eta, \quad (21)$$

$$\int_{T_k} \frac{\partial \psi_i^k}{\partial y}\,dxdy = \int_{T_{ref}} \left[-(A_2 + A_3\xi)\frac{\partial\lambda_i}{\partial\xi} + (A_1 + A_3\eta)\frac{\partial\lambda_i}{\partial\eta}\right] d\xi d\eta. (22)$$

A.2. Influence of the grid

We wonder if the classical method could coincide with the method of projection presented in Section 3. In other words, we are looking for conditions which imply

$$\int_\Omega \Phi \mathrm{div}\, \mathbf{v}_j \, dxdy = \int_\Omega \Pi_h \Phi \mathrm{div}\, \mathbf{v}_j \, dxdy, \tag{23}$$

with $\mathbf{v}_j = (v_j, 0)$ or $(0, v_j)$ for all the node j of the grid.

Proposition 1
If the elements of the mesh are identical rectangles whose sides are parallel to the coordinates axes, and if $\Phi(x,y) = \Psi_1(x) + \Psi_2(y) + \beta(x,y)$, where Ψ_1 and Ψ_2 denote two arbitrary functions and β is an arbitrary bilinear application (or, more generally, if Φ satisfies the property (15) of Section 3), then the classical method coincides with the projection method presented in Section 3.

Proof.
Let us consider the four quadrilaterals T_k, k=1,..,4 surrounding the node j. In order to simplify the notations we number them as on Figure 9. This allows us to write

$$v_j|_{T_k} = \psi_k^k$$

and for the sake of simplicity we denote ψ_k^k by ψ_k, forgetting the superscript k in the sequel.

Since we use the P0 finite elements space for the pressure, $\Pi_h \Phi$ is constant over each T_k. By definition $\Pi_h \Phi|_{T_k} = \Phi_k = \dfrac{1}{|T_k|} \displaystyle\int_{T_{ref}} \Phi \circ F_k(\xi, \eta) J \, d\xi d\eta$.

Taking $\mathbf{v}_j = (v_j, 0)$ we have :

$$\begin{aligned} \int_\Omega \Pi_h \Phi \frac{\partial v_j}{\partial x} \, dxdy &= \sum_{k=1}^4 \Phi_k \int_{T_k} \frac{\partial \psi_k}{\partial x} \, dxdy \\ &= \sum_{k=1}^4 \Phi_k \int_{T_{ref}} \left[(B_2^k + B_3^k \xi) \frac{\partial \lambda_k}{\partial \xi} - (B_1^k + B_3^k \eta) \frac{\partial \lambda_k}{\partial \eta} \right] d\xi d\eta, \end{aligned}$$

and

$$\begin{aligned} \int_\Omega \Phi \frac{\partial v_j}{\partial x} \, dxdy &= \sum_{k=1}^4 \int_{T_k} \Phi \frac{\partial \psi_k}{\partial x} \, dxdy \\ &= \sum_{k=1}^4 \int_{T_{ref}} \Phi \circ F_k(\xi, \eta) \left[(B_2^k + B_3^k \xi) \frac{\partial \lambda_k}{\partial \xi} - (B_1^k + B_3^k \eta) \frac{\partial \lambda_k}{\partial \eta} \right] d\xi d\eta. \end{aligned}$$

Let us now suppose that the quadrilaterals of the mesh are *parallelograms*. Then $A_3^k = 0$, $B_3^k = 0$ for all k, and $\Phi_k = \displaystyle\int_{T_{ref}} \Phi \circ F_k(\xi,\eta)\, d\xi d\eta$. Doing the same calculus with $\mathbf{v}_j = (0, v_j)$, equation (23) is finally equivalent to :

$$\left\{ \begin{array}{l} \displaystyle\sum_{k=1}^{4} (-1)^k \int_{T_{ref}} \Phi \circ F_k(\xi,\eta) \left[-A_1^k(\xi - \frac{1}{2}) + A_2^k(\eta - \frac{1}{2}) \right] d\xi d\eta = 0 \\ \displaystyle\sum_{k=1}^{4} (-1)^k \int_{T_{ref}} \Phi \circ F_k(\xi,\eta) \left[-B_1^k(\xi - \frac{1}{2}) + B_2^k(\eta - \frac{1}{2}) \right] d\xi d\eta = 0. \end{array} \right. \tag{24}$$

Let us write these equalities on the parallelograms T_k :

$$\left\{ \begin{array}{l} \displaystyle\sum_{k=1}^{4} \frac{(-1)^k}{|T_k|^2} \int_{T_k} \Phi(x,y) \left[2A_1^k A_2^k (y - y_c^k) - (B_1^k A_2^k + A_1^k B_2^k)(x - x_c^k) \right] dxdy = 0 \\ \displaystyle\sum_{k=1}^{4} \frac{(-1)^k}{|T_k|^2} \int_{T_k} \Phi(x,y) \left[2B_1^k B_2^k (x - x_c^k) - (B_1^k A_2^k + A_1^k B_2^k)(y - y_c^k) \right] dxdy = 0, \end{array} \right. \tag{25}$$

where (x_c^k, y_c^k) are the coordinates of the center C_k of T_k.

At last, if the quadrilaterals are *rectangles* whose sides are parallel to the coordinates axes, we have $A_2^k = B_1^k = 0$ for all k and (25) becomes :

$$\left\{ \begin{array}{lcl} \displaystyle\sum_{k=1}^{4} \frac{(-1)^k}{|T_k|} \int_{T_k} \Phi(x,y)(x - x_c^k)\, dxdy & = & 0 \\ \displaystyle\sum_{k=1}^{4} \frac{(-1)^k}{|T_k|} \int_{T_k} \Phi(x,y)(y - y_c^k)\, dxdy & = & 0 \end{array} \right. \tag{26}$$

When all the rectangles are identical, this relation is satisfied in particular by $\Phi(x,y) = \Psi_1(x) + \Psi_2(y) + \beta(x,y)$ where Ψ_1 and Ψ_2 are any functions and β an arbitrary bilinear form. Therefore, with forces $\mathbf{f}(x,y) = (f_1(x) + \alpha_1 y, f_2(y) + \alpha_2 x)$ formulations (10) and (13) are equivalent on meshes whose elements are identical and rectangular.

Appendix B

Our aim is to show that the projection method of Section 4 is more precise than the classical method in the case $\mathbf{f} = \nabla \Phi$.

We denote by $\mathbf{u}_h^c$ the velocity obtained with the classical method and $\mathbf{u}_h^p$ the velocity obtained by the projection method. We recall that the expected solution is $\mathbf{u} = 0$ and

$$\int_\Omega |\nabla \mathbf{u}_h^c|^2 \, dx = -\frac{1}{\eta} \int_\Omega \Phi \mathrm{div}\, \mathbf{u}_h^c \, dx, \tag{27}$$

whereas

$$\int_\Omega |\nabla \mathbf{u}_h^p|^2 \, dx = \frac{1}{\eta} \int_\Omega (\mathbf{f} - \nabla \Phi_h).\mathbf{u}_h^p \, dx = \frac{1}{\eta} \int_\Omega (\Phi_h - \Phi) \mathrm{div}\, \mathbf{u}_h^p \, dx. \tag{28}$$

B.1. Notations

For any $h > 0$, we denote by $\mathcal{T}_h$ a regular "triangulation" of $\overline{\Omega}$ of typical size h. We suppose here that any element $T \in \mathcal{T}_h$ is a quadrilateral, but it is not necessary.

As in Appendix A, T_{ref} is the reference unit square $[0,1] \times [0,1]$, F_T is the bilinear mapping that maps T_{ref} onto any quadrilateral T. We denote by Q_k the space of all polynomials in the reference space of the form $\hat{q}(\xi, \eta) = \sum c_{ij} \xi^i \eta^j$ where the sum range over all integers i and j such that $0 \leq i, j \leq k$. We define $Q_k(T) = \{q = \hat{q} \circ F_T^{-1}; \hat{q} \in Q_k\}$.

We introduce

$$\begin{aligned}
X_h &= \{\mathbf{v}_h \in \mathcal{C}^0(\overline{\Omega})^2; \mathbf{v}_h|_T \in Q_k(T)^2, \forall T \in \mathcal{T}_h\} \cap H_0^1(\Omega)^2, \\
M_h &= \{q_h \in L^2(\Omega); q_h|_T \in Q_l(T)^2, \forall T \in \mathcal{T}_h\} \cap L_0^2(\Omega), \\
Y_h &= \{y \in \mathcal{C}^0(\overline{\Omega}); y|_T \in Q_k(T), \forall T \in \mathcal{T}_h\} \cap L_0^2(\Omega).
\end{aligned}$$

The space X_h is devoted to the velocity, M_h to the pressure and Y_h to the potential part of the force $\mathbf{f}$.

We provide $H^m(\Omega)$ with the following seminorm

$$|v|_m = \left(\sum_{|\alpha| = m} \int_\Omega |D^\alpha v|^2 \, dx \right)^{1/2}.$$

For $\mathbf{f} = \nabla \Phi$ with $\Phi \in H^{m+1}(\Omega) \cap L_0^2(\Omega)$, $m \geq 0$ we define $\Phi_h \in Y_h$ as the finite element solution of the Neumann problem

$$\begin{aligned}
-\triangle \Phi &= \mathrm{div}\, \mathbf{f} \qquad \text{in } \Omega \\
\frac{\partial \Phi}{\partial \mathbf{n}} &= \mathbf{f}.\mathbf{n} \qquad \text{on } \partial\Omega.
\end{aligned}$$

such that $\int_\Omega \Phi_h = 0$ (the condition on $\partial\Omega$ is formal when $m = 0$). More precisely, we have :

$$\int_\Omega \nabla\Phi_h.\nabla\psi_h \, dx = \int_\Omega \mathbf{f}.\nabla\psi_h \, dx$$

for all $\psi_h \in Y_h$.

For $l \geq 0$ and for $z \in L_0^2(\Omega)$, we recall that $\Pi_h z \in M_h$ is defined as follows :

$$\Pi_h z|_T \in Q_l(T)$$

$$\int_T (\Pi_h z - z) q \, dx = 0 \qquad \forall q \in Q_l(T)$$

B.2. Error estimates

Proposition 2
We suppose that the force is a gradient $f = \nabla\Phi$ and we use the Q1/P0 pair of finite elements space. Then, when the typical size of the mesh h tends to zero, the seminorm $|.|_1$ of the velocity calculated by the classical method tends to zero like h whereas the velocity calculated by the projection method tends to zero like h^2.

Proof.

First, we recall the approximation result (see V. Girault and P.-A. Raviart [2] for instance) :

Lemma 1 *Let $\Phi \in H^{m+1}(\Omega)$, for some m such that $0 \leq m \leq k$. If we define Φ_h as described in B.1 we have :*

$$|\Phi - \Phi_h|_1 \leq C_1 h^m |\Phi|_{m+1},$$

with a constant $C_1 > 0$ independent of h and Φ.

The following lemma is a straightforward application of a result of projection in $L^2(\Omega)$ presented in [2] :

Lemma 2 *Let $z \in H^s(\Omega) \cap L_0^2(\Omega)$ for some s such that $0 \leq s \leq l+1$. The projection Π_h defined in B.1 satisfies :*

$$||z - \Pi_h z||_{L^2(\Omega)} \leq C_2 h^s |z|_s,$$

with a constant $C_2 > 0$ independent of h and z.

We restrict ourselves to the case $k = 1$, $l = 0$ corresponding to the pair Q1/P0. We choose $s = 1$ and $m = 1$ in the previous lemmata. In view of (27) we have :

$$
\begin{aligned}
|\mathbf{u}_h^c|_1^2 &= -\frac{1}{\eta}\int_\Omega (\Phi - \Pi_h\Phi)\mathrm{div}\,\mathbf{u}_h^c\,dx \\
&\leq \frac{1}{\eta}||\Phi - \Pi_h\Phi||_{L^2(\Omega)}||\mathrm{div}\,\mathbf{u}_h^c||_{L^2(\Omega)} \\
&\leq \frac{C_2}{\eta}h|\Phi|_1||\mathrm{div}\,\mathbf{u}_h^c||_{L^2(\Omega)}
\end{aligned}
$$

We deduce that

$$
|\mathbf{u}_h^c|_1 \leq \frac{C_2}{\eta}|\Phi|_1 h \tag{29}
$$

Whereas from (28) the estimate of $|u_h^p|_1$ is :

$$
\begin{aligned}
|\mathbf{u}_h^p|_1^2 &= -\frac{1}{\eta}\int_\Omega [(\Phi_h - \Phi) - \Pi_h(\Phi_h - \Phi)]\mathrm{div}\,\mathbf{u}_h^p\,dx \\
&\leq \frac{1}{\eta}||(\Phi_h - \Phi) - \Pi_h(\Phi_h - \Phi)||_{L^2(\Omega)}||\mathrm{div}\,\mathbf{u}_h^p||_{L^2(\Omega)} \\
&\leq \frac{C_2}{\eta}h|\Phi_h - \Phi|_1||\mathrm{div}\,\mathbf{u}_h^p||_{L^2(\Omega)} \\
&\leq \frac{C_1C_2}{\eta}h^2|\Phi|_2||\mathrm{div}\,\mathbf{u}_h^p||_{L^2(\Omega)}
\end{aligned}
$$

Thus :

$$
|\mathbf{u}_h^p|_1 \leq \frac{C_1C_2}{\eta}|\Phi|_2 h^2 \tag{30}
$$

A comparison between (29) and (30) shows the improvement of the projection method in the case of $\mathbf{f} = \nabla\Phi$. These estimates may be better in some peculiar cases (see Table 5).

		Classical method	Projection method
Experiment 1.2	Rectangular elements	0.1e-11	0.08e-11
($\mathbf{f} = cste$)	Distorted elements	0.83	0.2e-11
Experiment 1.3	Rectangular elements	0.76e-3	0.7e-12
($\mathbf{f} = \nabla\Phi_1$)	Distorted elements	0.17e-1	0.2e-12

Table 1: Maximum velocities (m/s) with the classical method and the projection method when $\mathbf{f} = \nabla\Phi$ with the Q1/P0 pair of finite elements.

		Classical method	Projection method
Experiment 1.2	Rectangular elements	0.2e-11	0.2e-11
($\mathbf{f} = cste$)	Distorted elements	0.3	0.5e-8
Experiment 1.3	Rectangular elements	0.4e-3	0.1e-11
($\mathbf{f} = \nabla\Phi_1$)	Distorted elements	0.14e-1	0.3e-10

Table 2: Same case as Table 1 with the Q2/P1 pair of finite elements.

		Classical method	Projection method for arbitrary $\mathbf{f}$
Experiment 1.2	Rectangular elements	0.1e-11	0.1e-11
($\mathbf{f} = cste$)	Distorted elements	0.83	0.2e-11
Experiment 1.3	Rectangular elements	0.76e-3	0.19e-5
($\mathbf{f} = \nabla\Phi_1$)	Distorted elements	0.17e-1	0.4e-3

Table 3: Maximum velocities (m/s) with the classical method and the projection method for arbitrary $\mathbf{f}$ with the Q1/P0 pair of finite elements.

		Classical method	Projection method for arbitrary $\mathbf{f}$
Experiment 1.2 ($\mathbf{f} = cste$)	Rectangular elements	0.9e-12	0.44e-11
	Distorted elements	0.3	0.14e-10
Experiment 1.3 ($\mathbf{f} = \nabla\Phi_1$)	Rectangular elements	0.4e-3	0.7e-7
	Distorted elements	0.14e-1	0.25e-4

Table 4: Same case as Table 3 with the Q2/P1 pair of finite elements.

h	Classical method	Projection method
0.067	6.49e-4	2.7e-6
0.05	3.66e-4	8.6e-7
0.033	1.63e-4	1.7e-7
0.028	1.19e-4	9.2e-8

Table 5: Value of $||\mathbf{u}_h||_{L^2(\Omega)^2}$ when the step of mesh h decreases (case $\mathbf{f} = \nabla\Phi_1$) with Q1/P0 elements.

h	Classical method	Projection method
0.083	2.1e-4	1.9e-7
0.067	0.86e-4	5.1e-8
0.05	0.28e-4	0.9e-8
0.045	0.19e-4	0.5e-8

Table 6: Same case as Table 5 with Q2/P1 elements.

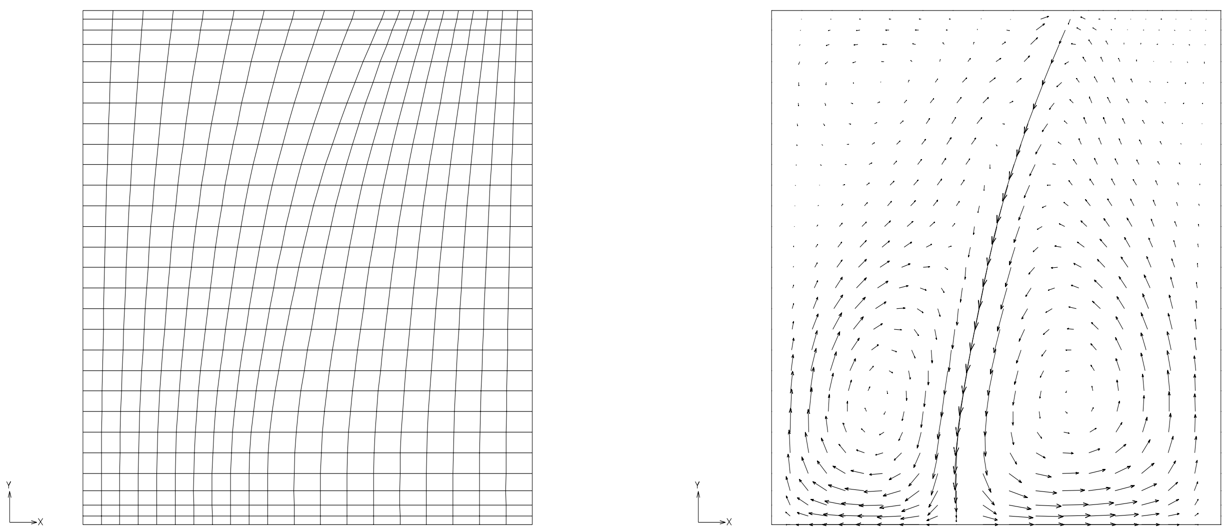

Figure 1: Spurious velocity (0.2 m/s) in two immiscible fluids submitted to $f = \nabla \Phi_0$ with $\Phi_0(x,y) = \frac{5}{2}y^2 - 10x$. On the left hand side : the mesh, on the right hand side : the velocity field. This test is performed with FIDAP V7.52 with the Q1/P0 pair of finite elements.

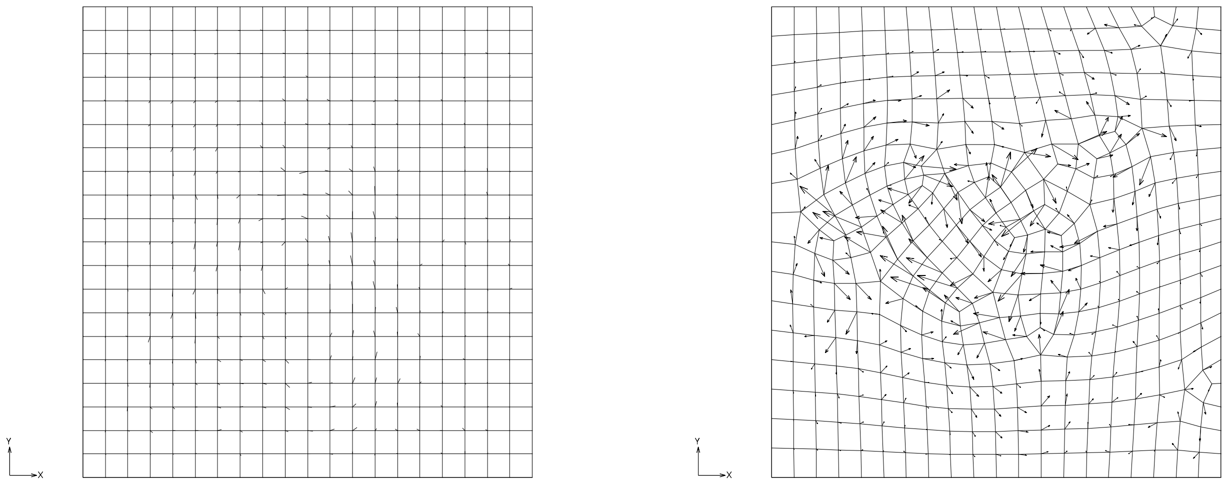

Figure 2: One fluid in presence of a constant force with the Q1/P0 elements. The influence of the shape of the mesh is striking : on the left hand side, maximum speed is 0.1e-11m/s, whereas it is 0.83 m/s on the right hand side.

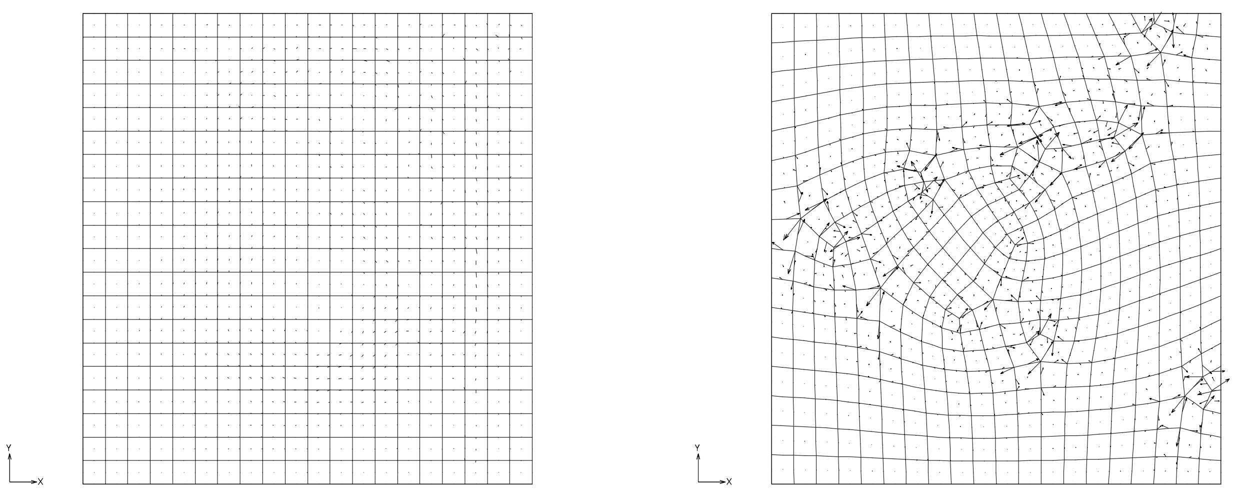

Figure 3: Same test as in Figure 2 with Q2/P1 elements. On the left hand side, maximum speed is 0.2e-11m/s. On the right hand side : 0.3m/s .

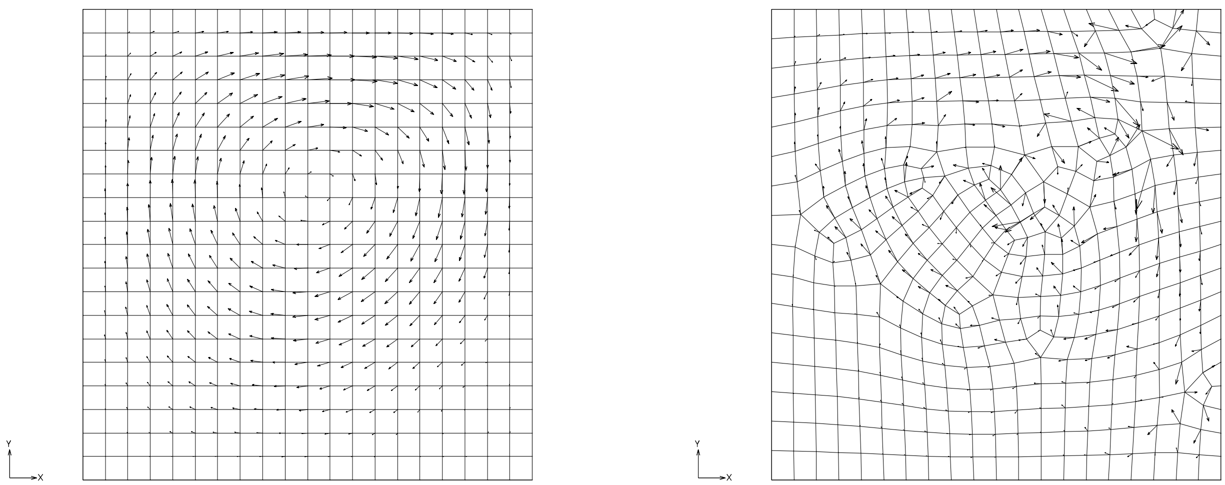

Figure 4: One fluid in presence of $\mathbf{f} = \nabla\Phi_1$. On the rectangular mesh, the speed reaches 0.76e-3m/s. On the bent mesh, 0.19e-1m/s. This case is presented with the Q1/P0 pair of finite elements. We obtain similar results with the Q2/P1 elements.

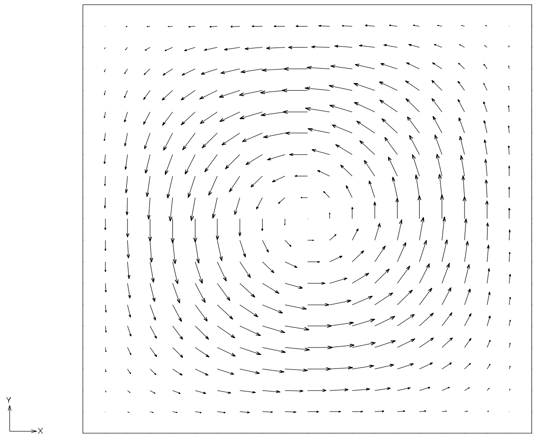

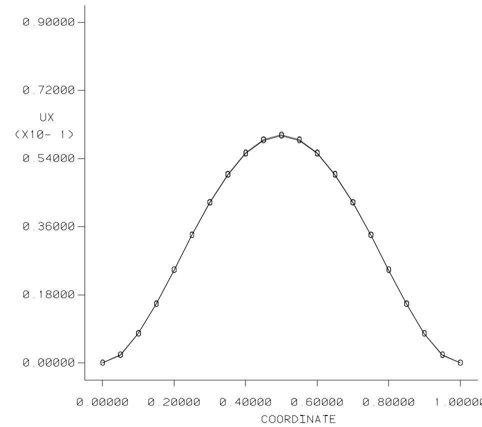

Figure 5: One fluid in presence of $\mathbf{f} = \nabla\Phi_0 + \mathbf{curl}\ g_0$ on *rectangular* elements. Left hand side : the velocity field. Right hand side : comparison between the theoretical first component of the velocity and the numerical one on the straight line $y = 0.4$. Finite elements : Q1/P0.

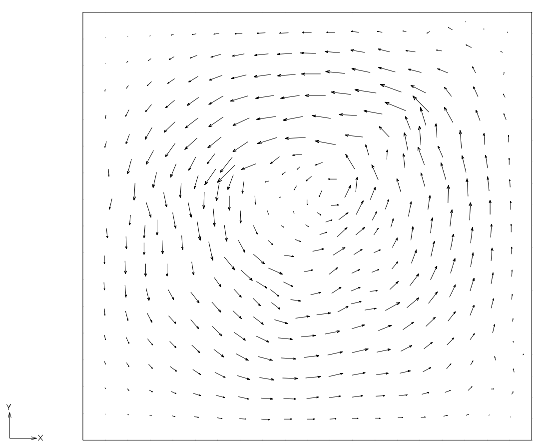

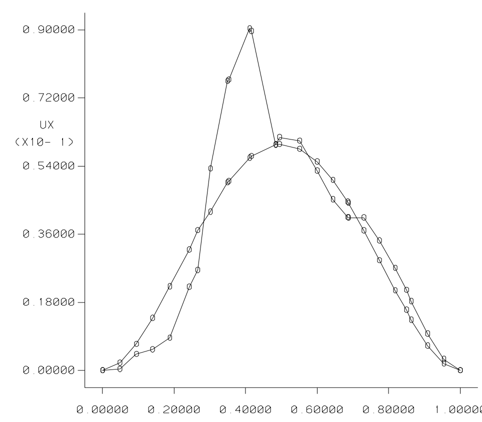

Figure 6: Same situation as Figure 5, but on a *distorted* mesh.

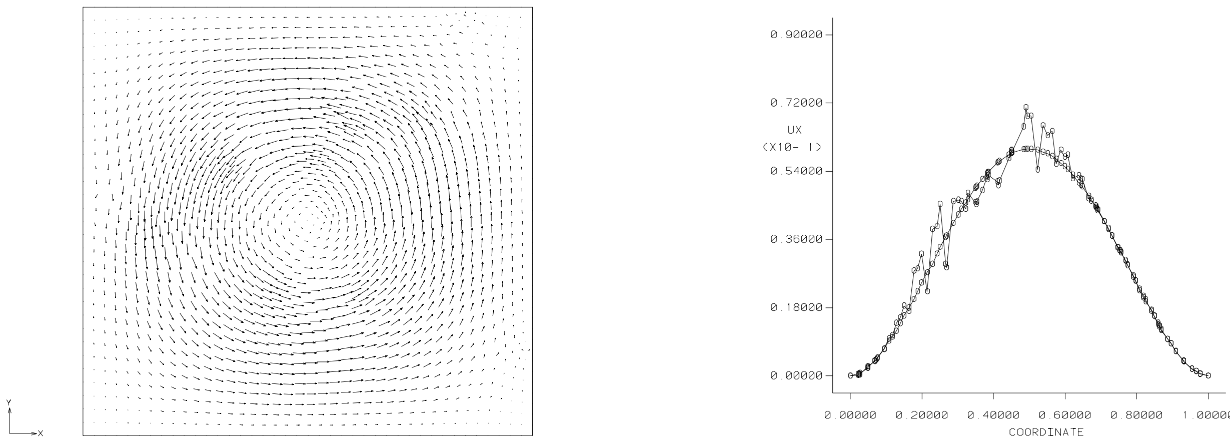

Figure 7: Same situation as Figure 6 (distorted mesh), but with Q2/P1 elements. While the Q2/P1 approximation is better than the Q1/P0, significant inaccuracies remain.

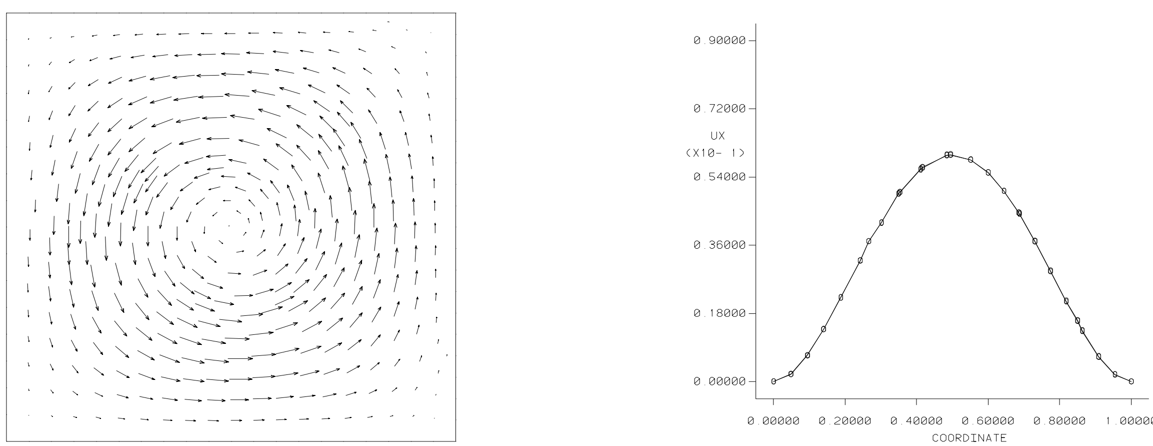

Figure 8: The projection method for the experiment 1.4 on the same distorted mesh as Figure 6. Note that the theoretical curve and the numerical one are now the same. A very precise result is also obtained by the projection method with the Q2/P1 elements in the case corresponding to Figure 7.

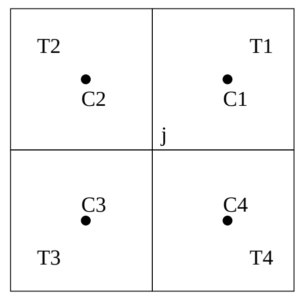

Figure 9: The four elements around the node j.

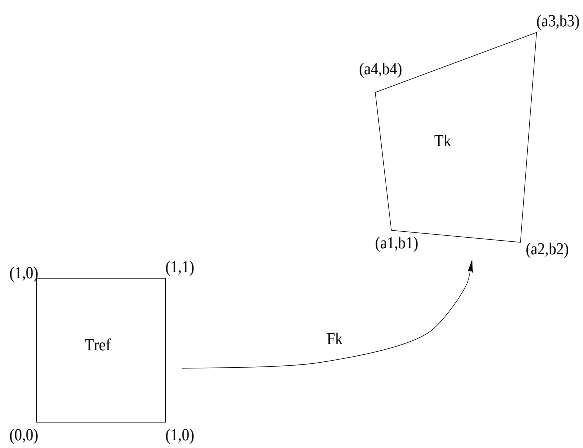

Figure 10: Quadrilateral T_k and reference unit square T_{ref}.